

Pion momentum distributions in Minkowski space.

Wayne de Paula

Instituto Tecnológico de Aeronáutica - Brasil

Collaborators

Abigail Castro (ITA), Giovanni Salmè (INFN), Tobias Frederico (ITA), Emanuel Ydrefors (IMP-Lanzhou)

Nonperturbative QFT in the complex momentum space - 2023
Maynooth University



Summary

- 1 Overview
- 2 Pion as a quark-antiquark bound state
- 3 Observables
 - LF Momentum Distributions
 - Em form factor and charge radius
 - Transverse Momentum-Dependent Distributions (TMDs)
- 4 Dressed quark propagator
- 5 Conclusions and Perspectives

Overview

Most non-perturbative methods for QCD are formulated in Euclidean space, since the indefinite metric of the Minkowski space generates many difficulties.

Overview

Most non-perturbative methods for QCD are formulated in Euclidean space, since the indefinite metric of the Minkowski space generates many difficulties.

The primary tool for investigating QCD in Euclidean space is the lattice, but relevant advancements have been achieved with a continuum approach.

Overview

Most non-perturbative methods for QCD are formulated in Euclidean space, since the indefinite metric of the Minkowski space generates many difficulties.

The primary tool for investigating QCD in Euclidean space is the lattice, but relevant advancements have been achieved with a continuum approach.

The continuum approach is based on the combination of the Bethe-Salpeter equation (BSE) for two and three-body systems (Faddeev-BSE), and the set of Dyson-Schwinger equations (DSEs).

Overview

Most non-perturbative methods for QCD are formulated in Euclidean space, since the indefinite metric of the Minkowski space generates many difficulties.

The primary tool for investigating QCD in Euclidean space is the lattice, but relevant advancements have been achieved with a continuum approach.

The continuum approach is based on the combination of the Bethe-Salpeter equation (BSE) for two and three-body systems (Faddeev-BSE), and the set of Dyson-Schwinger equations (DSEs).

Results of the hadron spectra and dynamical observables have been favorably compared with available experimental results and lattice calculations.

Overview

Most non-perturbative methods for QCD are formulated in Euclidean space, since the indefinite metric of the Minkowski space generates many difficulties.

The primary tool for investigating QCD in Euclidean space is the lattice, but relevant advancements have been achieved with a continuum approach.

The continuum approach is based on the combination of the Bethe-Salpeter equation (BSE) for two and three-body systems (Faddeev-BSE), and the set of Dyson-Schwinger equations (DSEs).

Results of the hadron spectra and dynamical observables have been favorably compared with available experimental results and lattice calculations.

BUT the physical observations are obtained in Minkowski space, and therefore, it could be helpful to attempt to replicate in Minkowski space an analog program: i.e. combining BSE and a truncated tower of DSEs.

Overview

Most non-perturbative methods for QCD are formulated in Euclidean space, since the indefinite metric of the Minkowski space generates many difficulties.

The primary tool for investigating QCD in Euclidean space is the lattice, but relevant advancements have been achieved with a continuum approach.

The continuum approach is based on the combination of the Bethe-Salpeter equation (BSE) for two and three-body systems (Faddeev-BSE), and the set of Dyson-Schwinger equations (DSEs).

Results of the hadron spectra and dynamical observables have been favorably compared with available experimental results and lattice calculations.

BUT the physical observations are obtained in Minkowski space, and therefore, it could be helpful to attempt to replicate in Minkowski space an analog program: i.e. combining BSE and a truncated tower of DSEs.

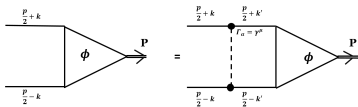
⇒ The approach we are pursuing is based on using the Nakanishi Integral Representation to calculate observables in Minkowski space.

Pion as a quark-antiquark bound state

Bethe-Salpeter equation (0^-) :

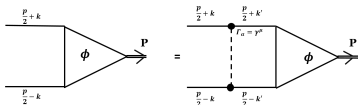
Pion as a quark-antiquark bound state

Bethe-Salpeter equation (0^-) :



Pion as a quark-antiquark bound state

Bethe-Salpeter equation (0^-) :



$$\Phi(k; P) = S(k + \frac{P}{2}) \int \frac{d^4 k'}{(2\pi)^4} S^{\mu\nu}(q) \Gamma_\mu(q) \Phi(k'; P) \hat{\Gamma}_\nu(q) S(k - \frac{P}{2})$$

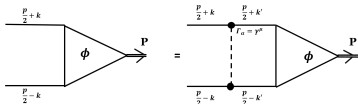
$$\hat{\Gamma}_\nu(q) = C \Gamma_\nu(q) C^{-1}$$

where we use: i) bare propagators for the quarks and gluons;
 ii) ladder approximation with massive gluons,
 iii) an extended quark-gluon vertex

$$S(P) = \frac{i}{\not{P} - m + i\epsilon}, \quad S^{\mu\nu}(q) = -i \frac{g^{\mu\nu}}{q^2 - \mu^2 + i\epsilon}, \quad \Gamma^\mu = ig \frac{\mu^2 - \Lambda^2}{q^2 - \Lambda^2 + i\epsilon} \gamma^\mu,$$

Pion as a quark-antiquark bound state

Bethe-Salpeter equation (0^-) :



$$\Phi(k; P) = S(k + \frac{P}{2}) \int \frac{d^4 k'}{(2\pi)^4} S^{\mu\nu}(q) \Gamma_\mu(q) \Phi(k'; P) \hat{\Gamma}_\nu(q) S(k - \frac{P}{2})$$

$$\hat{\Gamma}_\nu(q) = C \Gamma_\nu(q) C^{-1}$$

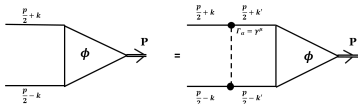
where we use: i) bare propagators for the quarks and gluons;
 ii) ladder approximation with massive gluons,
 iii) an extended quark-gluon vertex

$$S(P) = \frac{i}{\not{P} - m + i\epsilon}, \quad S^{\mu\nu}(q) = -i \frac{g^{\mu\nu}}{q^2 - \mu^2 + i\epsilon}, \quad \Gamma^\mu = ig \frac{\mu^2 - \Lambda^2}{q^2 - \Lambda^2 + i\epsilon} \gamma^\mu,$$

We consider one of the Longitudinal components of the QGV

Pion as a quark-antiquark bound state

Bethe-Salpeter equation (0^-) :



$$\Phi(k; P) = S(k + \frac{P}{2}) \int \frac{d^4 k'}{(2\pi)^4} S^{\mu\nu}(q) \Gamma_\mu(q) \Phi(k'; P) \hat{\Gamma}_\nu(q) S(k - \frac{P}{2})$$

$$\hat{\Gamma}_\nu(q) = C \Gamma_\nu(q) C^{-1}$$

where we use: i) bare propagators for the quarks and gluons;
 ii) ladder approximation with massive gluons,
 iii) an extended quark-gluon vertex

$$S(P) = \frac{i}{\not{P} - m + i\epsilon}, \quad S^{\mu\nu}(q) = -i \frac{g^{\mu\nu}}{q^2 - \mu^2 + i\epsilon}, \quad \Gamma^\mu = ig \frac{\mu^2 - \Lambda^2}{q^2 - \Lambda^2 + i\epsilon} \gamma^\mu,$$

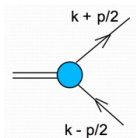
We consider one of the Longitudinal components of the QGV

We set the value of the scale parameter (300 MeV) from the combined analysis of Lattice simulations, the Quark-Gap Equation and Slanov-Taylor identity.

Oliveira, WP, Frederico, de Melo EPJC 78(7), 553 (2018) & EPJC 79 (2019) 116 & EPJC 80 (2020) 484

NIR for fermion-antifermion 0^- Bound State

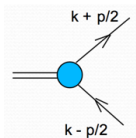
BSA for a quark-antiquark 0^- bound state:



$$\Phi(k; P) = \sum_{i=1}^4 S_i(k; P) \phi_i(k; P)$$

NIR for fermion-antifermion 0^- Bound State

BSA for a quark-antiquark 0^- bound state:

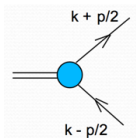


$$\Phi(k; P) = \sum_{i=1}^4 S_i(k; P) \phi_i(k; P)$$

Dirac structures for a pseudoscalar system is given by

NIR for fermion-antifermion 0^- Bound State

BSA for a quark-antiquark 0^- bound state:



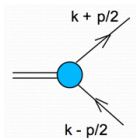
$$\Phi(k; P) = \sum_{i=1}^4 S_i(k; P) \phi_i(k; P)$$

Dirac structures for a pseudoscalar system is given by

$$S_1 = \gamma_5, S_2 = \frac{P}{M} \gamma_5, S_3 = \frac{k \cdot P}{M^3} P \gamma_5 - \frac{k}{M} \gamma_5, S_4 = \frac{i}{M^2} \sigma^{\mu\nu} P_\mu k_\nu \gamma_5$$

NIR for fermion-antifermion 0^- Bound State

BSA for a quark-antiquark 0^- bound state:



$$\Phi(k; P) = \sum_{i=1}^4 S_i(k; P) \phi_i(k; P)$$

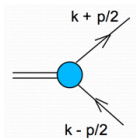
Dirac structures for a pseudoscalar system is given by

$$S_1 = \gamma_5, S_2 = \frac{P}{M} \gamma_5, S_3 = \frac{k \cdot P}{M^3} P \gamma_5 - \frac{k}{M} \gamma_5, S_4 = \frac{i}{M^2} \sigma^{\mu\nu} P_\mu k_\nu \gamma_5$$

Using the NIR for each scalar functions

NIR for fermion-antifermion 0^- Bound State

BSA for a quark-antiquark 0^- bound state:



$$\Phi(k; P) = \sum_{i=1}^4 S_i(k; P) \phi_i(k; P)$$

Dirac structures for a pseudoscalar system is given by

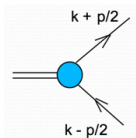
$$S_1 = \gamma_5, S_2 = \frac{P}{M} \gamma_5, S_3 = \frac{k \cdot P}{M^3} \not{P} \gamma_5 - \frac{k}{M} \gamma_5, S_4 = \frac{i}{M^2} \sigma^{\mu\nu} P_\mu k_\nu \gamma_5$$

Using the NIR for each scalar functions

$$\phi_i(k; P) = \int_{-1}^1 dz' \int_0^\infty d\gamma' \frac{g_i(\gamma', z'; \kappa^2)}{[k^2 + z'(P \cdot k) - \gamma' - \kappa^2 + i\epsilon]^3}$$

NIR for fermion-antifermion 0^- Bound State

BSA for a quark-antiquark 0^- bound state:



$$\Phi(k; P) = \sum_{i=1}^4 S_i(k; P) \phi_i(k; P)$$

Dirac structures for a pseudoscalar system is given by

$$S_1 = \gamma_5, S_2 = \frac{P}{M} \gamma_5, S_3 = \frac{k \cdot P}{M^3} P \gamma_5 - \frac{k}{M} \gamma_5, S_4 = \frac{i}{M^2} \sigma^{\mu\nu} P_\mu k_\nu \gamma_5$$

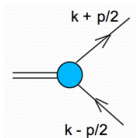
Using the NIR for each scalar functions

$$\phi_i(k; P) = \int_{-1}^1 dz' \int_0^\infty d\gamma' \frac{g_i(\gamma', z'; \kappa^2)}{[k^2 + z'(P \cdot k) - \gamma' - \kappa^2 + i\epsilon]^3}$$

System of coupled integral equations

NIR for fermion-antifermion 0^- Bound State

BSA for a quark-antiquark 0^- bound state:



$$\Phi(k; P) = \sum_{i=1}^4 S_i(k; P) \phi_i(k; P)$$

Dirac structures for a pseudoscalar system is given by

$$S_1 = \gamma_5, S_2 = \frac{P}{M} \gamma_5, S_3 = \frac{k \cdot P}{M^3} \not{P} \gamma_5 - \frac{k}{M} \gamma_5, S_4 = \frac{i}{M^2} \sigma^{\mu\nu} P_\mu k_\nu \gamma_5$$

Using the NIR for each scalar functions

$$\phi_i(k; P) = \int_{-1}^1 dz' \int_0^\infty d\gamma' \frac{g_i(\gamma', z'; \kappa^2)}{[k^2 + z'(P \cdot k) - \gamma' - \kappa^2 + i\epsilon]^3}$$

System of coupled integral equations

$$\int_{-1}^1 dz' \int_0^\infty d\gamma' \frac{g_i(\gamma', z')}{[k^2 + z'p \cdot k - \gamma' - \kappa^2 + i\epsilon]^3} = \sum_j \int_{-1}^1 dz' \int_0^\infty d\gamma' \mathcal{K}_{ij}(k, p; \gamma', z') g_j(\gamma', z')$$

Projecting BSE onto the LF hyper-plane $x^+ = 0$

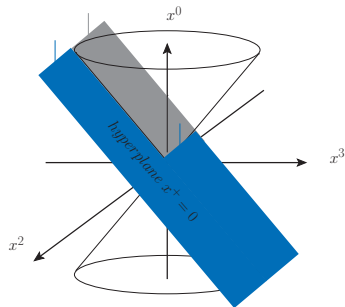
Projecting BSE onto the LF hyper-plane $x^+ = 0$

Light-Front variables: $x^\mu = (x^+, x^-, \vec{x}_\perp)$

$$\text{LF-time } x^+ = x^0 + x^3$$

$$x^- = x^0 - x^3$$

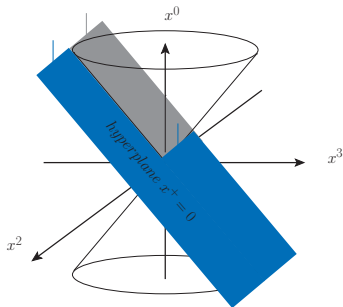
$$\vec{x}_\perp = (x^1, x^2)$$



Projecting BSE onto the LF hyper-plane $x^+ = 0$

Light-Front variables: $x^\mu = (x^+, x^-, \vec{x}_\perp)$

$$\begin{aligned}\text{LF-time } x^+ &= x^0 + x^3 \\ x^- &= x^0 - x^3 \\ \vec{x}_\perp &= (x^1, x^2)\end{aligned}$$

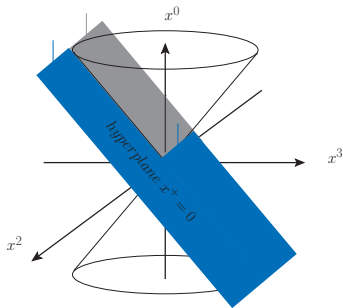


Within the LF framework, one introduces LF-projected amplitudes for each $\phi_i(k, P)$ through their integral on k^- (\Rightarrow s.t. $x^+ = 0$, with x^+ relative LF-time):

Projecting BSE onto the LF hyper-plane $x^+ = 0$

Light-Front variables: $x^\mu = (x^+, x^-, \vec{x}_\perp)$

$$\begin{aligned}\text{LF-time } x^+ &= x^0 + x^3 \\ x^- &= x^0 - x^3 \\ \vec{x}_\perp &= (x^1, x^2)\end{aligned}$$



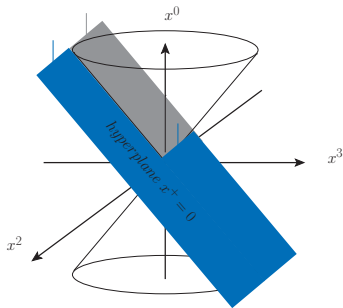
Within the LF framework, one introduces LF-projected amplitudes for each $\phi_i(k, P)$ through their integral on k^- (\Rightarrow s.t. $x^+ = 0$, with x^+ relative LF-time):

$$\psi_i(\gamma, \xi) = \int \frac{dk^-}{2\pi} \phi_i(k, p) = -\frac{i}{M} \int_0^\infty d\gamma' \frac{g_i(\gamma', z; \kappa^2)}{[\gamma + \gamma' + m^2 z^2 + (1 - z^2)\kappa^2]^2}$$

Projecting BSE onto the LF hyper-plane $x^+ = 0$

Light-Front variables: $x^\mu = (x^+, x^-, \vec{x}_\perp)$

$$\begin{aligned}\text{LF-time } x^+ &= x^0 + x^3 \\ x^- &= x^0 - x^3 \\ \vec{x}_\perp &= (x^1, x^2)\end{aligned}$$



Within the LF framework, one introduces LF-projected amplitudes for each $\phi_i(k, P)$ through their integral on k^- (\Rightarrow s.t. $x^+ = 0$, with x^+ relative LF-time)):

$$\psi_i(\gamma, \xi) = \int \frac{dk^-}{2\pi} \phi_i(k, p) = -\frac{i}{M} \int_0^\infty d\gamma' \frac{g_i(\gamma', z; \kappa^2)}{[\gamma + \gamma' + m^2 z^2 + (1 - z^2)\kappa^2]^2}$$

By LF-projecting both sides of BSE (after applying the suitable traces on Dirac indexes) one gets a **coupled integral-equation system**.

The coupled integral-equation system (see also NIR+covariant LF, Carbonell and Karmanov JPA 2010) in ladder approximation, reads (cf. de Paula, et al, PRD **94**, 071901 (2016) & EPJC **77**, 764 (2017))

$$\int_0^\infty \frac{d\gamma' g_i(\gamma', z; \kappa^2)}{[\gamma + \gamma' + m^2 z^2 + (1 - z^2)\kappa^2]^2} = iMg^2 \sum_j \int_0^\infty d\gamma' \int_{-1}^1 dz' \mathcal{L}_{ij}(\gamma, z; \gamma', z') g_j(\gamma', z'; \kappa^2)$$

In ladder approximation, the Nakanishi Kernel, \mathcal{L}_{ij} , has an analytical expression and contains **singular contributions** that can be regularized 'a la Yan (Chang and Yan, Quantum field theories in the infinite momentum frame. II. PRD **7**, 1147 (1973)).

Numerical solutions are obtained by discretizing the system using a **polynomial basis**, given by the **Cartesian product of Laguerre(γ) \times Gegenbauer(z)**. One remains with a Generalized eigenvalue problem, where a non-symmetric matrix and a symmetric one are present

$$A \vec{c} = \lambda B \vec{c}$$

N.B. the eigenvector \vec{c} contains the coefficients of the expansion of the Nakanishi weight functions $g_i(z, \gamma; \kappa^2)$.

LF Momentum Distributions

LF Momentum Distributions

The fermionic field on the null-plane is given by:

$$\psi^{(+)}(\tilde{x}, x^+ = 0^+) = \int \frac{d\tilde{q}}{(2\pi)^{3/2}} \frac{\theta(q^+)}{\sqrt{2q^+}} \sum_{\sigma} \left[U^{(+)}(\tilde{q}, \sigma) b(\tilde{q}, \sigma) e^{i\tilde{q} \cdot \tilde{x}} + V^{(+)}(\tilde{q}, \sigma) d^{\dagger}(\tilde{q}, \sigma) e^{-i\tilde{q} \cdot \tilde{x}} \right],$$

where

$$U^{(+)}(\tilde{q}, \sigma) = \Lambda^+ u(\tilde{q}, \sigma) \quad , \quad V^{(+)}(\tilde{q}, \sigma) = \Lambda^+ v(\tilde{q}, \sigma)$$

Hence, d^{\dagger} and b are the fermion creation/annihilation operators

LF Momentum Distributions

The fermionic field on the null-plane is given by:

$$\psi^{(+)}(\tilde{x}, x^+ = 0^+) = \int \frac{d\tilde{q}}{(2\pi)^{3/2}} \frac{\theta(q^+)}{\sqrt{2q^+}} \sum_{\sigma} \left[U^{(+)}(\tilde{q}, \sigma) b(\tilde{q}, \sigma) e^{i\tilde{q} \cdot \tilde{x}} + V^{(+)}(\tilde{q}, \sigma) d^{\dagger}(\tilde{q}, \sigma) e^{-i\tilde{q} \cdot \tilde{x}} \right],$$

where

$$U^{(+)}(\tilde{q}, \sigma) = \Lambda^+ u(\tilde{q}, \sigma) \quad , \quad V^{(+)}(\tilde{q}, \sigma) = \Lambda^+ v(\tilde{q}, \sigma)$$

Hence, d^{\dagger} and b are the fermion creation/annihilation operators

The LF valence amplitude is the Fock component with the lowest number of constituents:

LF Momentum Distributions

The fermionic field on the null-plane is given by:

$$\psi^{(+)}(\tilde{x}, x^+ = 0^+) = \int \frac{d\tilde{q}}{(2\pi)^{3/2}} \frac{\theta(q^+)}{\sqrt{2q^+}} \sum_{\sigma} \left[U^{(+)}(\tilde{q}, \sigma) b(\tilde{q}, \sigma) e^{i\tilde{q}\cdot\tilde{x}} + V^{(+)}(\tilde{q}, \sigma) d^{\dagger}(\tilde{q}, \sigma) e^{-i\tilde{q}\cdot\tilde{x}} \right],$$

where

$$U^{(+)}(\tilde{q}, \sigma) = \Lambda^+ u(\tilde{q}, \sigma) \quad , \quad V^{(+)}(\tilde{q}, \sigma) = \Lambda^+ v(\tilde{q}, \sigma)$$

Hence, d^{\dagger} and b are the fermion creation/annihilation operators

The **LF valence amplitude** is the **Fock component** with the lowest number of constituents:

$$\varphi_2(\xi, \mathbf{k}_{\perp}, \sigma_i; M, J^{\pi}, J_z) = (2\pi)^3 \sqrt{N_c} 2p^+ \sqrt{\xi(1-\xi)} \langle 0 | b(\tilde{q}_2, \sigma_2) d(\tilde{q}_1, \sigma_1) | \bar{p}, M, J^{\pi}, J_z \rangle ,$$

where $\tilde{q}_1 \equiv \{q_1^+ = M(1-\xi), -\mathbf{k}_{\perp}\}$, $\tilde{q}_2 \equiv \{q_2^+ = M\xi, \mathbf{k}_{\perp}\}$ and $\xi = 1/2 + k^+/p^+$.

LF Momentum Distributions

LF Momentum Distributions

LF valence amplitude in terms of BS amplitude is:

$$\varphi_2(\xi, \mathbf{k}_\perp, \sigma_j; M, J^\pi, J_z) = \frac{\sqrt{N_c}}{p^+} \frac{1}{4} \bar{u}_\alpha(\tilde{q}_2, \sigma_2) \int \frac{dk^-}{2\pi} [\gamma^+ \Phi(k, p) \gamma^+]_{\alpha\beta} v_\beta(\tilde{q}_1, \sigma_1) .$$

LF Momentum Distributions

LF valence amplitude in terms of BS amplitude is:

$$\varphi_2(\xi, \mathbf{k}_\perp, \sigma_j; M, J^\pi, J_z) = \frac{\sqrt{N_c}}{p^+} \frac{1}{4} \bar{u}_\alpha(\tilde{q}_2, \sigma_2) \int \frac{dk^-}{2\pi} [\gamma^+ \Phi(k, p) \gamma^+]_{\alpha\beta} v_\beta(\tilde{q}_1, \sigma_1) .$$

which can be decomposed into two spin contributions:

LF Momentum Distributions

LF valence amplitude in terms of BS amplitude is:

$$\varphi_2(\xi, \mathbf{k}_\perp, \sigma_i; M, J^\pi, J_z) = \frac{\sqrt{N_c}}{p^+} \frac{1}{4} \bar{u}_\alpha(\tilde{q}_2, \sigma_2) \int \frac{dk^-}{2\pi} [\gamma^+ \Phi(k, p) \gamma^+]_{\alpha\beta} v_\beta(\tilde{q}_1, \sigma_1) .$$

which can be decomposed into two spin contributions:

Anti-aligned configuration:

$$\psi_{\uparrow\downarrow}(\gamma, z) = \psi_2(\gamma, z) + \frac{z}{2} \psi_3(\gamma, \xi) + \frac{i}{M^3} \int_0^\infty d\gamma' \frac{\partial g_3(\gamma', z)/\partial z}{\gamma + \gamma' + z^2 m^2 + (1 - z^2) \kappa^2}$$

LF Momentum Distributions

LF valence amplitude in terms of BS amplitude is:

$$\varphi_2(\xi, \mathbf{k}_\perp, \sigma_i; M, J^\pi, J_z) = \frac{\sqrt{N_c}}{p^+} \frac{1}{4} \bar{u}_\alpha(\bar{q}_2, \sigma_2) \int \frac{dk^-}{2\pi} [\gamma^+ \Phi(k, p) \gamma^+]_{\alpha\beta} v_\beta(\bar{q}_1, \sigma_1) .$$

which can be decomposed into two spin contributions:

Anti-aligned configuration:

$$\psi_{\uparrow\downarrow}(\gamma, z) = \psi_2(\gamma, z) + \frac{z}{2} \psi_3(\gamma, \xi) + \frac{i}{M^3} \int_0^\infty d\gamma' \frac{\partial g_3(\gamma', z)/\partial z}{\gamma + \gamma' + z^2 m^2 + (1 - z^2) \kappa^2}$$

Aligned configuration:

$$\psi_{\uparrow\uparrow}(\gamma, z) = \psi_{\downarrow\downarrow}(\gamma, z) = \frac{\sqrt{\gamma}}{M} \psi_4(\gamma, z)$$

LF Momentum Distributions

LF valence amplitude in terms of BS amplitude is:

$$\varphi_2(\xi, \mathbf{k}_\perp, \sigma_i; M, J^\pi, J_z) = \frac{\sqrt{N_c}}{p^+} \frac{1}{4} \bar{u}_\alpha(\bar{q}_2, \sigma_2) \int \frac{dk^-}{2\pi} [\gamma^+ \Phi(k, p) \gamma^+]_{\alpha\beta} v_\beta(\bar{q}_1, \sigma_1) .$$

which can be decomposed into two spin contributions:

Anti-aligned configuration:

$$\psi_{\uparrow\downarrow}(\gamma, z) = \psi_2(\gamma, z) + \frac{z}{2} \psi_3(\gamma, \xi) + \frac{i}{M^3} \int_0^\infty d\gamma' \frac{\partial g_3(\gamma', z)/\partial z}{\gamma + \gamma' + z^2 m^2 + (1 - z^2) \kappa^2}$$

Aligned configuration:

$$\psi_{\uparrow\uparrow}(\gamma, z) = \psi_{\downarrow\downarrow}(\gamma, z) = \frac{\sqrt{\gamma}}{M} \psi_4(\gamma, z)$$

with the LF amplitudes given by

$$\psi_i(\gamma, z) = -\frac{i}{M} \int_0^\infty d\gamma' \frac{g_i(\gamma', z)}{[\gamma + \gamma' + m^2 z^2 + (1 - z^2) \kappa^2]^2}$$

Valence probability

Valence probability

The Fock expansion allows to restore a probabilistic framework.

The Valence Probability is:

$$P_{val} = \frac{1}{(2\pi)^3} \sum_{\sigma_1 \sigma_2} \int_{-1}^1 \frac{dz}{(1-z^2)} \int d\mathbf{k}_\perp \left| \varphi_{n=2}(\xi, \mathbf{k}_\perp, \sigma_i; M, J^\pi, J_z) \right|^2$$

Valence probability

The Fock expansion allows to restore a probabilistic framework.

The Valence Probability is:

$$P_{val} = \frac{1}{(2\pi)^3} \sum_{\sigma_1 \sigma_2} \int_{-1}^1 \frac{dz}{(1-z^2)} \int d\mathbf{k}_\perp \left| \varphi_{n=2}(\xi, \mathbf{k}_\perp, \sigma_i; M, J^\pi, J_z) \right|^2$$

In terms of the aligned and anti-aligned LFWF, we have

$$P_{val} = \int_{-1}^1 dz \int_0^\infty \frac{d\gamma}{(4\pi)^2} \left[|\psi_{\uparrow\downarrow}(\gamma, z)|^2 + |\psi_{\uparrow\uparrow}(\gamma, z)|^2 \right],$$

Valence probability

The Fock expansion allows to restore a probabilistic framework.

The Valence Probability is:

$$P_{val} = \frac{1}{(2\pi)^3} \sum_{\sigma_1 \sigma_2} \int_{-1}^1 \frac{dz}{(1-z^2)} \int d\mathbf{k}_\perp \left| \varphi_{n=2}(\xi, \mathbf{k}_\perp, \sigma_i; M, J^\pi, J_z) \right|^2$$

In terms of the aligned and anti-aligned LFWF, we have

$$P_{val} = \int_{-1}^1 dz \int_0^\infty \frac{d\gamma}{(4\pi)^2} \left[|\psi_{\uparrow\downarrow}(\gamma, z)|^2 + |\psi_{\uparrow\uparrow}(\gamma, z)|^2 \right],$$

The contribution to the PDF from the LF-valence WF is

$$u_{val}(z) = \int_0^\infty \frac{d\gamma}{(4\pi)^2} \left[|\psi_{\uparrow\downarrow}(\gamma, z)|^2 + |\psi_{\uparrow\uparrow}(\gamma, z)|^2 \right]$$

Quantitative results: Static properties

WP, Ydrefors, Nogueira, Frederico and Salme PRD 103 014002 (2021).

Quantitative results: Static properties

WP, Ydrefors, Nogueira, Frederico and Salme PRD 103 014002 (2021).

Set	m (MeV)	B/m	μ/m	Λ/m	P_{val}	$P_{\uparrow\downarrow}$	$P_{\uparrow\uparrow}$	f_π (MeV)
I	187	1.25	0.15	2	0.64	0.55	0.09	77
II	255	1.45	1.5	1	0.65	0.55	0.10	112
III	255	1.45	2	1	0.66	0.56	0.11	117
IV	215	1.35	2	1	0.67	0.57	0.11	98
V	187	1.25	2	1	0.67	0.56	0.11	84
VI	255	1.45	2.5	1	0.68	0.56	0.11	122
VII	255	1.45	2.5	1.1	0.69	0.56	0.12	127
VIII	255	1.45	2.5	1.2	0.70	0.57	0.13	130
IX	255	1.45	1	2	0.70	0.57	0.14	134
X	215	1.35	1	2	0.71	0.57	0.14	112
XI	187	1.25	1	2	0.71	0.58	0.14	96

Quantitative results: Static properties

WP, Ydrefors, Nogueira, Frederico and Salme PRD 103 014002 (2021).

Set	m (MeV)	B/m	μ/m	Λ/m	P_{val}	$P_{\uparrow\downarrow}$	$P_{\uparrow\uparrow}$	f_π (MeV)
I	187	1.25	0.15	2	0.64	0.55	0.09	77
II	255	1.45	1.5	1	0.65	0.55	0.10	112
III	255	1.45	2	1	0.66	0.56	0.11	117
IV	215	1.35	2	1	0.67	0.57	0.11	98
V	187	1.25	2	1	0.67	0.56	0.11	84
VI	255	1.45	2.5	1	0.68	0.56	0.11	122
VII	255	1.45	2.5	1.1	0.69	0.56	0.12	127
VIII	255	1.45	2.5	1.2	0.70	0.57	0.13	130
IX	255	1.45	1	2	0.70	0.57	0.14	134
X	215	1.35	1	2	0.71	0.57	0.14	112
XI	187	1.25	1	2	0.71	0.58	0.14	96

The set VIII reproduces the **pion decay constant**

$$m_q = 255 \text{ MeV}, m_g = 637.5 \text{ MeV} \text{ and } \Lambda = 306 \text{ MeV}$$

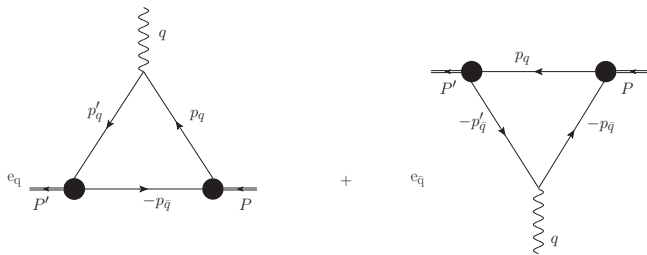
The contributions **beyond the valence** component are important, $\sim 30\%$

Pion em form factor in ladder approximation

Ydrefors, WP, Nogueira, Frederico and Salmè PLB 820, 136494 (2021)

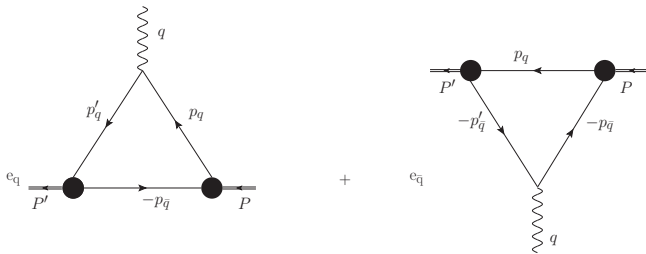
Pion em form factor in ladder approximation

Ydrefors, WP, Nogueira, Frederico and Salmè PLB 820, 136494 (2021)



Pion em form factor in ladder approximation

Ydrefors, WP, Nogueira, Frederico and Salmè PLB 820, 136494 (2021)



The elastic FF is given by

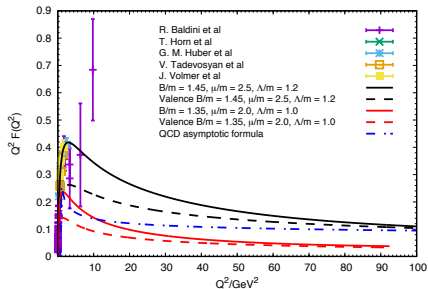
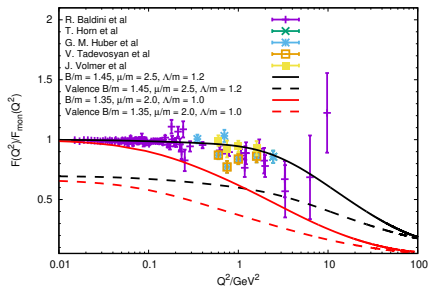
$$F(Q^2) = -i \frac{N_c}{M^2 (1 + \tau)} \int \frac{d^4 p_{\bar{q}}}{(2\pi)^4} \text{Tr} [(-\not{p}_{\bar{q}} - m) \bar{\Phi}(k'; P') (\not{P} + \not{P}') \Phi(k; P)]$$

Pion em form factor in ladder approximation

Ydrefors, WP, Nogueira, Frederico and Salmè PLB 820, 136494 (2021)

Pion em form factor in ladder approximation

Ydrefors, WP, Nogueira, Frederico and Salmè PLB 820, 136494 (2021)



$$m_q = 255\text{MeV}, m_g = 637\text{MeV} \text{ and } \Lambda = 306\text{MeV}$$

Good agreement with experimental data (black solid curve).

For high Q^2 we obtain the valence dominance (dashed black curve)

Right Panel: Dash-dotted line; asymptotic expression from Brodsky-Lepage PRD

22 (1980): $Q^2 F_{\text{asy}}(Q^2) = 8\pi\alpha_s(Q^2)f_\pi^2$. Our results recover the pQCD for large

Q^2

Pion charge radius

Ydrefors, WP, Nogueira, Frederico and Salmè PLB 820, 136494 (2021)

Pion charge radius

Ydrefors, WP, Nogueira, Frederico and Salmè PLB 820, 136494 (2021)

Pion charge radius and its decomposition in valence and non valence contributions.

Set	m	B/m	μ/m	Λ/m	P_{val}	f_π	r_π (fm)	r_{val} (fm)	r_{nval} (fm)
I	255	1.45	2.5	1.2	0.70	130	0.663	0.710	0.538
II	215	1.35	2	1	0.67	98	0.835	0.895	0.703

$$\text{where } r_\pi^2 = -6 \left. \frac{dF_\pi(Q^2)}{dQ^2} \right|_{Q^2=0}$$

$$P_{val(nval)} r_{val(nval)}^2 = -6 \left. \frac{dF_{val(nval)}(Q^2)}{dQ^2} \right|_{Q^2=0}$$

Pion charge radius

Ydrefors, WP, Nogueira, Frederico and Salmè PLB 820, 136494 (2021)

Pion charge radius and its decomposition in valence and non valence contributions.

Set	m	B/m	μ/m	Λ/m	P_{val}	f_π	r_π (fm)	r_{val} (fm)	r_{nval} (fm)
I	255	1.45	2.5	1.2	0.70	130	0.663	0.710	0.538
II	215	1.35	2	1	0.67	98	0.835	0.895	0.703

where $r_\pi^2 = -6 \left. dF_\pi(Q^2)/dQ^2 \right|_{Q^2=0}$

$P_{val(nval)} r_{val(nval)}^2 = -6 \left. dF_{val(nval)}(Q^2)/dQ^2 \right|_{Q^2=0}$

The set I is in fair agreement with the PDG value:

$$r_\pi^{PDG} = 0.659 \pm 0.004 \text{ fm}$$

Pion Transverse Momentum-Dependent Distributions

One can define the T-even subleading quark uTMDs, starting from the decomposition of the pion correlator (Mulders and Tangerman, Nucl. Phys. B 461, 197 (1996)).

twist -2 uTMD:

$$f_1^q(\gamma, \xi) = \frac{N_c}{4} \int d\phi_{\hat{\mathbf{k}}_\perp} \int_{-\infty}^{\infty} \frac{dy^- d\mathbf{y}_\perp}{2(2\pi)^3} e^{i[\tilde{\mathbf{k}} \cdot \tilde{\mathbf{y}}]} \langle P | \bar{\psi}_q(-\frac{y}{2}) \hat{1} \psi_q(\frac{y}{2}) | P \rangle \Big|_{y^+=0}$$

twist-3 uTMD

$$\frac{M}{P^+} e^q(\gamma, \xi) = \frac{N_c}{4} \int d\phi_{\hat{\mathbf{k}}_\perp} \int_{-\infty}^{\infty} \frac{dy^- d\mathbf{y}_\perp}{2(2\pi)^3} e^{i[\tilde{\mathbf{k}} \cdot \tilde{\mathbf{y}}]} \langle P | \bar{\psi}_q(-\frac{y}{2}) \gamma^+ \psi_q(\frac{y}{2}) | P \rangle \Big|_{y^+=0}$$

and

$$\frac{M}{P^+} f^{\perp q}(\gamma, \xi) = \frac{N_c M}{4|\mathbf{k}_\perp|^2} \int d\phi_{\hat{\mathbf{k}}_\perp} \int_{-\infty}^{\infty} \frac{dy^- d\mathbf{y}_\perp}{2(2\pi)^3} e^{i[\tilde{\mathbf{k}} \cdot \tilde{\mathbf{y}}]} \langle P | \bar{\psi}_q(-\frac{y}{2}) \mathbf{k}_\perp \cdot \boldsymbol{\gamma}_\perp \psi_q(\frac{y}{2}) | P \rangle \Big|_{y^+=0}$$

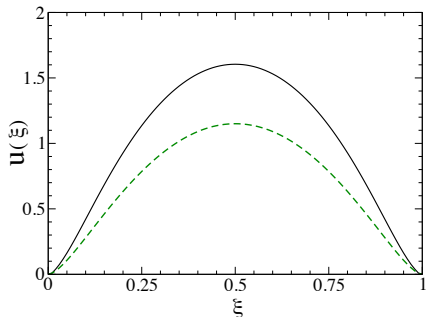
with $\tilde{\mathbf{k}} \cdot \tilde{\mathbf{y}} = \xi P^+ y^- / 2 - \mathbf{k}_\perp \cdot \mathbf{y}_\perp$.

Parton distribution function

W. de Paula et al., PRD **105**, L071505 (2022).

From the charge-symmetric expression for the leading-twist TMD $f_1^S(\gamma, \xi)$, one gets the PDF at the initial scale $u(\xi)$

$$f_1^{S(AS)}(\gamma, \xi) = \frac{f_1^q(\gamma, \xi) \pm f_1^{\bar{q}}(\gamma, 1 - \xi)}{2} \Rightarrow u(\xi) = \int_0^\infty d\gamma f_1^S(\gamma, \xi).$$



Solid line: full calculation of the BSE at the model scale

Dashed line: The LF valence contribution .

At the initial scale, for $\xi \rightarrow 1$, the exponent of $(1 - \xi)^{\eta_0}$ is $\eta_0 = 1.4$. N.B JAM collaboration (PRL **121** (2018)) found a preferential exponent $\eta_{JAM} \sim 1$.

Parton distribution function II

Low order Mellin moments at scales $Q = 2.0$ GeV and $Q = 5.2$ GeV.

	BSE ₂	LQCD ₂	BSE ₅	LQCD ₅
$\langle x \rangle$	0.259	0.261 ± 0.007	0.221	0.229 ± 0.008
$\langle x^2 \rangle$	0.105	0.110 ± 0.014	0.082	0.087 ± 0.009
$\langle x^3 \rangle$	0.052	0.024 ± 0.018	0.039	0.042 ± 0.010
$\langle x^4 \rangle$	0.029		0.021	0.023 ± 0.009
$\langle x^5 \rangle$	0.018		0.012	0.014 ± 0.007
$\langle x^6 \rangle$	0.012		0.008	0.009 ± 0.005

LQCD, $Q = 2.0$ GeV: $\langle x \rangle$ - Alexandrou et al PRD 103, 014508 (2021)
 $\langle x^2 \rangle$ and $\langle x^3 \rangle$ - Alexandrou et al PRD 104, 054504 (2021)

LQCD, $Q = 5.0$ GeV: $\langle x \rangle$ - Alexandrou et al PRD 103, 014508 (2021)

N.B. following Cui et al EPJC 2020 80 1064, lowest order DGLAP equations used for evolution. One needs:

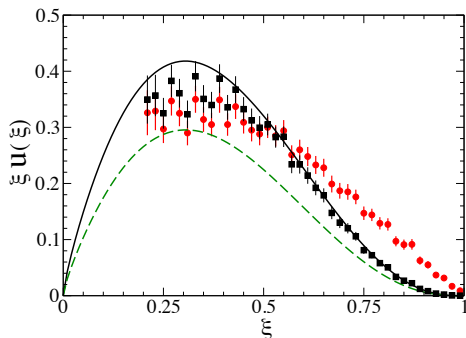
Hadronic scale and effective charge for dealing with DGLAP

$$Q_0 = 0.330 \pm 0.030 \text{ GeV}$$

Within the error, we choose $Q_0 = 0.360$ GeV to fit the first Mellin moment.

Parton distribution function III

Comparison with the data at 5.2 GeV scale



Solid line: full calculation of the BSE evolved from the initial scale $Q_0 = 0.360$ GeV to $Q = 5.2$ GeV

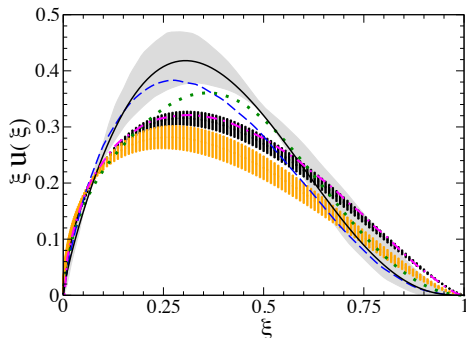
Dashed line: The evolved LF valence contribution

Full dots: experimental data from E615

Full squares: reanalyzed experimental data from Aicher et al PRL 105, 252003 (2010) evolved to $Q = 5.2$ GeV

Parton distribution function IV

Comparison with other theoretical calculations



Solid line: full calculation of the BSE evolved from the initial scale $Q_0 = 0.360$ GeV to $Q = 5.2$ GeV

Dashed line: DSE calculation from Cui et al, Eur. Phys. J. A 58, 10 (2022)

Dash-dotted line: DSE calculation with dressed quark-photon vertex from Bednar et al PRL 124, 042002 (2020)

Dotted line: BLFQ collaboration, PLB 825, 136890 (2022)

Gray area: LQCD results from C. Alexandrou et al (2021)

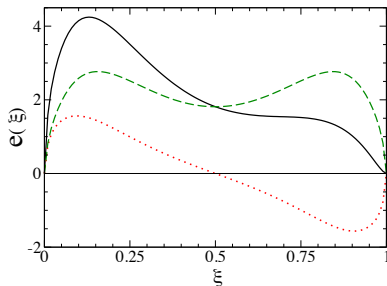
Black and Orange vertical lines from JAM collaboration, private communication.

For the evolved $\xi u(\xi)$, the exponent of $(1 - \xi)^{\eta_5}$ is $\eta_5 = 2.94$, when $\xi \rightarrow 1$,

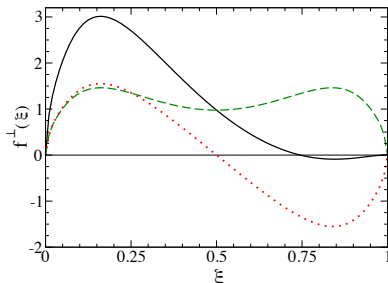
LQCD: Alexandrou et al PRD 104, 054504 (2021) obtained 2.20 ± 0.64

Cui et al EPJA 58, 10 (2022) obtained 2.81 ± 0.08

Transverse Momentum-Dependent Distributions II



Solid line: quark twist-3 uTMD $e(\xi)$
 Dashed line: Sym. twist-3 uTMD $e^S(\xi)$
 Dotted: AS twist-3 uTMD $e^{AS}(\xi)$

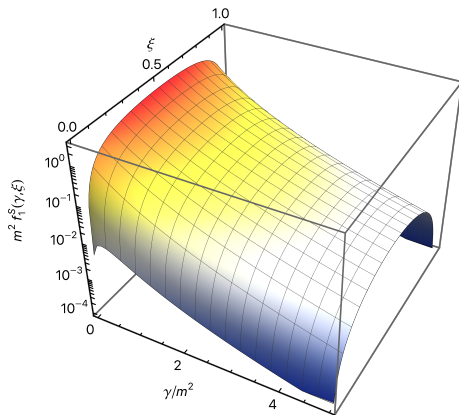


Solid line: quark twist-3 uTMD $f^\perp(\xi)$
 Dashed line: Sym. twist-3 uTMD $f^{\perp S}(\xi)$
 Dotted: AS twist-3 uTMD $f^{\perp AS}(\xi)$

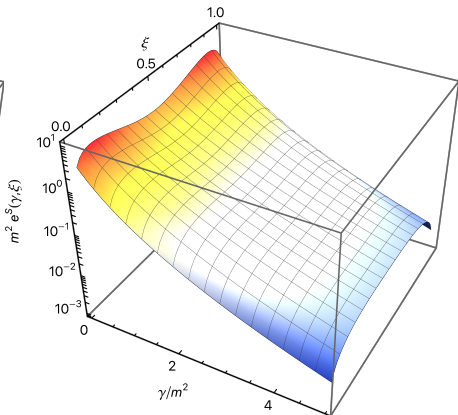
The corresponding symmetric and antisymmetric collinear PDFs are:

$$e^{S(AS)}(\xi) = \int_0^\infty d\gamma e^{S(AS)}(\gamma, \xi), \quad f^{\perp S(AS)}(\xi) = \int_0^\infty d\gamma f^{\perp S(AS)}(\gamma, \xi)$$

For the quark ones: $e^q(\xi) = e^S(\xi) + e^{AS}(\xi)$ and $f^{\perp q}(\xi) = f^{\perp S}(\xi) + f^{\perp AS}(\xi)$



Twist-2 uTMD $f_1^S(\gamma, \xi)$



Twist-3 uTMD $e^S(\gamma, \xi)$

Twist-2

- i) the peak at $\xi = 0.5$ for any γ/m^2
- ii) the vanishing values at the end-points
- iii) the order of magnitude fall-off already for $\gamma/m^2 > 2$

Similar behavior in comparison with DSE calculations (Shi, Bednar, Cloët, PRD 101(7), 074014 (2020))

Different behavior in comparison to "LF constituent model" (Pasquini, Schweitzer, PRD 90(1), 014050 (2014)) and "LF holographic models" (Bacchetta, Cotogno, Pasquini, PLB 771, 546 (2017).)

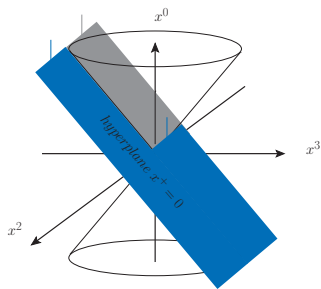
Twist-3

Double-hump: smooth for larger γ/m^2 .

A view of the pion from the light-cone

W. de Paula, et al, PRD 103, 014002 (2021) The probability distribution of the quarks inside the pion, sitting on the the hyperplane $x^+ = 0$, tangent to the light-cone, is evaluated in the space given by the Cartesian product of the *loffe-time* and the plane spanned by the transverse coordinates \mathbf{b}_\perp .

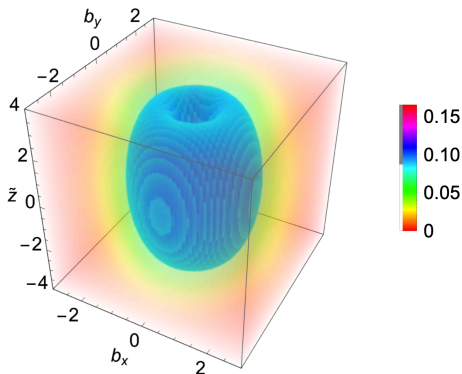
Why? In addition to the usual the infinite-momentum frame one can study the deep-inelastic scattering processes in the target frame, adopting the configuration space, so that a more detailed investigation of the space-time structure of the hadrons can be performed. The *loffe-time* is useful for studying the relative importance of short and long light-like distances.



The covariant definition of the loffe-time is $\tilde{z} = x \cdot P_{target}$, and it becomes $\tilde{z} = x^- P_{target}^+ / 2$ on the hyperplane $x^+ = 0$

The pion on the light-cone

Density plot of $|\mathbf{b}_\perp|^2 |\psi(\tilde{z}, b_x, b_y)|^2$, with $\psi(\tilde{z}, b_x, b_y)$ obtained from our solutions of the ladder Bethe-Salpeter equation [W. de Paula et al PRD 103, (2021) 014002]



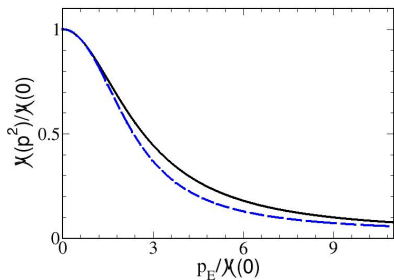
$\tilde{z} \equiv$ loffe-time

$\{b_x, b_y\} \equiv$ transverse coordinates

Dressed quark propagator

After completing the investigation of the pion BSE with **fixed-mass quark**, i.e. a $q\bar{q}$ bound system, we are addressing the **running-mass case**

Wave-function renorm. constant $Z(p^2) = 1$ and a running-mass, $\mathcal{M}(p_E^2) = m_0 - m^3/(p_E^2 - \lambda^2)$, with $m_0 = 0.008$ GeV, $m = 0.648$ GeV and $\lambda = 0.9$ GeV adjusted to LQCD calculations by O. Oliveira, et al, PRD **99** (2019) 094506. First results in A. Castro et al, arXiv:2305.12536



The **quark running-mass**, $\mathcal{M}(p^2)$, as a function of the Euclidean momentum $p_E = \sqrt{-p^2}$, in units of the IR mass $\mathcal{M}(0) = 0.344$ GeV. Solid line: our model. Dashed line: accurate fit of the LQCD calculations .

0^- Bound State with Running quark mass function

Abigail Castro, WP, Ydrefors, Frederico, Salmè - arXiv:2305.12536

0^- Bound State with Running quark mass function

Abigail Castro, WP, Ydrefors, Frederico, Salmè - arXiv:2305.12536

Dressed quark propagator: $S(p) = S^V(p^2)\not{p} + S^S(p^2)$

Integral Representation: $S^V(p^2) = \int_0^\infty ds \frac{\rho^V(s)}{p^2 - s + i\epsilon}$; $S^S(p^2) = \int_0^\infty ds \frac{\rho^S(s)}{p^2 - s + i\epsilon}$

0^- Bound State with Running quark mass function

Abigail Castro, WP, Ydrefors, Frederico, Salmè - arXiv:2305.12536

Dressed quark propagator: $S(p) = S^V(p^2)\not{p} + S^S(p^2)$

Integral Representation: $S^V(p^2) = \int_0^\infty ds \frac{\rho^V(s)}{p^2 - s + i\epsilon}$; $S^S(p^2) = \int_0^\infty ds \frac{\rho^S(s)}{p^2 - s + i\epsilon}$

Using the Nakanishi integral representation for $\phi_i(k, p)$, performing the loop integral and projecting onto the LF, one obtains the BSE as

0^- Bound State with Running quark mass function

Abigail Castro, WP, Ydrefors, Frederico, Salmè - arXiv:2305.12536

Dressed quark propagator: $S(p) = S^V(p^2)\not{p} + S^S(p^2)$

Integral Representation: $S^V(p^2) = \int_0^\infty ds \frac{\rho^V(s)}{p^2 - s + i\epsilon}$; $S^S(p^2) = \int_0^\infty ds \frac{\rho^S(s)}{p^2 - s + i\epsilon}$

Using the Nakanishi integral representation for $\phi_i(k, p)$, performing the loop integral and projecting onto the LF, one obtains the BSE as

$$\int_0^\infty d\gamma' \frac{g_i(\gamma', z)}{\left[\gamma + z^2 M^2/4 + \gamma' + \kappa^2 - i\epsilon\right]^2} = \frac{\alpha}{2\pi} \\ \times \sum_j \int_{-1}^1 dz' \int_0^\infty d\gamma' \mathcal{L}_{ij}(\gamma, z; \gamma', z') g_j(\gamma', z').$$

0^- Bound State with Running quark mass function

Abigail Castro, WP, Ydrefors, Frederico, Salmè - arXiv:2305.12536

Phenomenological model: $\mathcal{M}(p^2) = m_0 - \frac{m^3}{p^2 - \lambda^2 + i\epsilon}$

$$\rho^{S(V)}(s) = \sum_{a=1}^3 R_a^{S(V)} \delta(s - m_a^2),$$

where $R_a^{S(V)}$ are the **residues**, that read

$$R_a^V = \frac{(\lambda^2 - m_a^2)^2}{(m_a^2 - m_b^2)(m_a^2 - m_c^2)},$$

$$R_a^S = R_a^V \mathcal{M}(m_a^2),$$

with the indices $\{a, b, c\}$ following the cyclic permutation $\{1, 2, 3\}$.

$\mathcal{M}(0)$	i	m_i	R_i^V	R_i^S
[GeV]		[GeV]		[GeV]
	1	0.4696	3.7784	1.7743
0.344	2	0.5733	-2.8863	-1.6546
	3	1.0349	0.1079	-0.1116

0^- Bound State with Running quark mass function

Abigail Castro, WP, Ydrefors, Frederico, Salmè - arXiv:2305.12536

0^- Bound State with Running quark mass function

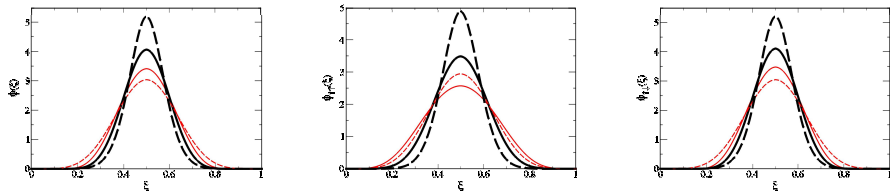
Abigail Castro, WP, Ydrefors, Frederico, Salmè - arXiv:2305.12536

Longitudinal momentum distribution

0^- Bound State with Running quark mass function

Abigail Castro, WP, Ydrefors, Frederico, Salmè - arXiv:2305.12536

Longitudinal momentum distribution



Parameters: $\Lambda = 0.12$ GeV, $\mu = 0.469$ GeV.

Thick solid line: running mass model for $M = 0.653$ GeV.

Thick dashed Line: fixed quark mass (344 MeV) for $M = 0.653$ GeV.

Thin solid line: running mass model for $M = 0.516$ GeV.

Thin dashed line: fixed quark mass (344 MeV) for $M = 0.516$ GeV.

0^- Bound State with Running quark mass function

Abigail Castro, WP, Ydrefors, Frederico, Salmè - arXiv:2305.12536

0^- Bound State with Running quark mass function

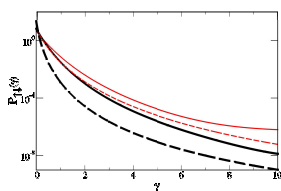
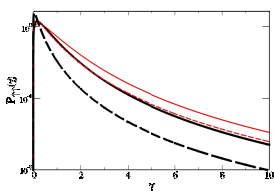
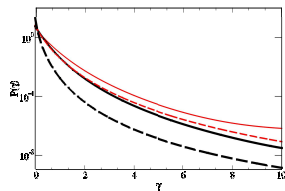
Abigail Castro, WP, Ydrefors, Frederico, Salmè - arXiv:2305.12536

Transverse momentum distribution

0^- Bound State with Running quark mass function

Abigail Castro, WP, Ydrefors, Frederico, Salmè - arXiv:2305.12536

Transverse momentum distribution



Parameters: $\Lambda = 0.12$ GeV, $\mu = 0.469$ GeV.

Thick solid line: running mass model for $M = 0.653$ GeV.

Thick dashed Line: fixed quark mass (344 MeV) for $M = 0.653$ GeV.

Thin solid line: running mass model for $M = 0.516$ GeV.

Thin dashed line: fixed quark mass (344 MeV) for $M = 0.516$ GeV.

Dressing the Quark: Schwinger-Dyson equation

Dressing the Quark: Schwinger-Dyson equation

The model: Bare vertices, massive vector boson, Pauli-Villars regulator

Dressing the Quark: Schwinger-Dyson equation

The model: Bare vertices, massive vector boson, Pauli-Villars regulator

Dressing the Quark: Schwinger-Dyson equation

The model: Bare vertices, massive vector boson, Pauli-Villars regulator

The diagram shows the Schwinger-Dyson equation for a quark propagator. On the left, a horizontal line with a black dot in the middle is labeled with 'p' above and '-1' to the right. This is followed by an equals sign. To the right of the equals sign is a bare propagator, represented by a horizontal line with an arrow pointing to the right, labeled with 'p' above and '-1' to the right. This is followed by a plus sign and a loop diagram. The loop diagram consists of a horizontal line with two black dots, labeled with 'k' below. A wavy line (representing a massive vector boson) connects the two dots, forming a semi-circular arc above the line. The wavy line is labeled with 'p-k' at its right end.

Dressing the Quark: Schwinger-Dyson equation

The model: Bare vertices, massive vector boson, Pauli-Villars regulator

$$S_q^{-1}(p) = S_q^{-1}(p) + \text{loop diagram}$$

The rainbow ladder Schwinger-Dyson equation in **Minkowski space** is:

$$S_q^{-1}(k) = \not{k} - m_B + ig^2 \int \frac{d^4 q}{(2\pi)^4} \Gamma_\mu(q, k) S_q(k - q) \gamma_\nu D^{\mu\nu}(q),$$

where m_B is the **quark bare mass** and g is the coupling constant.

Dressing the Quark: Schwinger-Dyson equation

The model: Bare vertices, massive vector boson, Pauli-Villars regulator

$$S_q^{-1}(p) = S_q^{-1}(p) + \text{loop diagram}$$

The rainbow ladder Schwinger-Dyson equation in **Minkowski space** is:

$$S_q^{-1}(k) = \not{k} - m_B + ig^2 \int \frac{d^4 q}{(2\pi)^4} \Gamma_\mu(q, k) S_q(k - q) \gamma_\nu D^{\mu\nu}(q),$$

where m_B is the **quark bare mass** and g is the coupling constant.

The massive gauge boson is given by

$$D^{\mu\nu}(q) = \frac{1}{q^2 - m_g^2 + i\epsilon} \left[g^{\mu\nu} - \frac{(1 - \xi)q^\mu q^\nu}{q^2 - \xi m_g^2 + i\epsilon} \right],$$

where we have introduced an effective gluon mass m_g , as suggested by LQCD calculations (see *Dudal, Oliveira and Silva, PRD 89 (2014) 014010*).

Dressing the Quark: Schwinger-Dyson equation

The model: Bare vertices, massive vector boson, Pauli-Villars regulator

$$S_q^{-1}(k) = S_q^{-1}(k) + \text{loop diagram}$$

The rainbow ladder Schwinger-Dyson equation in **Minkowski space** is:

$$S_q^{-1}(k) = \not{k} - m_B + ig^2 \int \frac{d^4 q}{(2\pi)^4} \Gamma_\mu(q, k) S_q(k - q) \gamma_\nu D^{\mu\nu}(q),$$

where m_B is the **quark bare mass** and g is the coupling constant.

The massive gauge boson is given by

$$D^{\mu\nu}(q) = \frac{1}{q^2 - m_g^2 + i\epsilon} \left[g^{\mu\nu} - \frac{(1 - \xi)q^\mu q^\nu}{q^2 - \xi m_g^2 + i\epsilon} \right],$$

where we have introduced an effective gluon mass m_g , as suggested by LQCD calculations (see *Dudal, Oliveira and Silva, PRD 89 (2014) 014010*).

The dressed fermion propagator is

$$S_q(k) = \left[\not{k} A(k^2) - B(k^2) + i\epsilon \right]^{-1}.$$

Schwinger-Dyson equation in Rainbow ladder truncation

The vector and scalar **self-energies** are given by the **KLR**, respectively as:

$$A(k^2) = 1 + \int_0^\infty ds \frac{\rho_A(s)}{k^2 - s + i\epsilon},$$
$$B(k^2) = m_B + \int_0^\infty ds \frac{\rho_B(s)}{k^2 - s + i\epsilon}.$$

Schwinger-Dyson equation in Rainbow ladder truncation

The vector and scalar **self-energies** are given by the **KLR**, respectively as:

$$A(k^2) = 1 + \int_0^\infty ds \frac{\rho_A(s)}{k^2 - s + i\epsilon},$$
$$B(k^2) = m_B + \int_0^\infty ds \frac{\rho_B(s)}{k^2 - s + i\epsilon}.$$

The quark propagator can also be written as:

$$S_q(k) = R \frac{\not{k} + \bar{m}_0}{k^2 - \bar{m}_0^2 + i\epsilon} + \not{k} \int_0^\infty ds \frac{\rho_v(s)}{k^2 - s + i\epsilon} + \int_0^\infty ds \frac{\rho_s(s)}{k^2 - s + i\epsilon},$$

where \bar{m}_0 is the **renormalized mass**.

Schwinger-Dyson equation in Rainbow ladder truncation

The vector and scalar **self-energies** are given by the **KLR**, respectively as:

$$A(k^2) = 1 + \int_0^\infty ds \frac{\rho_A(s)}{k^2 - s + i\epsilon},$$

$$B(k^2) = m_B + \int_0^\infty ds \frac{\rho_B(s)}{k^2 - s + i\epsilon}.$$

The quark propagator can also be written as:

$$S_q(k) = R \frac{\not{k} + \bar{m}_0}{k^2 - \bar{m}_0^2 + i\epsilon} + \not{k} \int_0^\infty ds \frac{\rho_v(s)}{k^2 - s + i\epsilon} + \int_0^\infty ds \frac{\rho_s(s)}{k^2 - s + i\epsilon},$$

where \bar{m}_0 is the **renormalized mass**.

$$\not{k}A(k^2) - B(k^2) = ig^2 \int \frac{d^4q}{(2\pi)^4} \frac{\gamma_\mu S_f(k-q)\gamma_\nu}{q^2 - m_g^2 + i\epsilon} \left[g^{\mu\nu} - \frac{(1-\xi)q^\mu q^\nu}{q^2 - \xi m_g^2 + i\epsilon} \right]$$

↖ **Gauge fixing**

$$- i g^2 \int \frac{d^4q}{(2\pi)^4} \frac{\gamma_\mu S_f(k-q)\gamma_\nu}{q^2 - \Lambda^2 + i\epsilon} \left[g^{\mu\nu} - \frac{(1-\xi)q^\mu q^\nu}{q^2 - \xi \Lambda^2 + i\epsilon} \right]$$

← **Pauli-Villars regulator**

Phenomenological Model

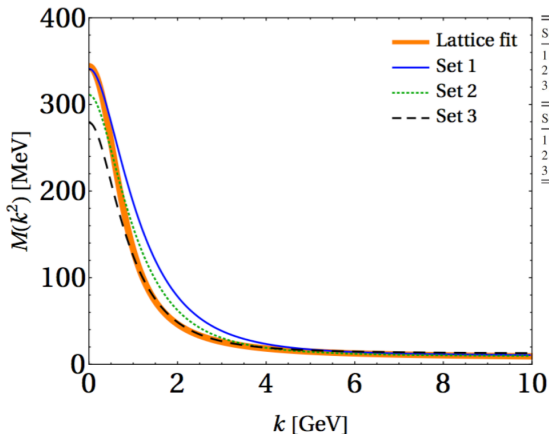
Duarte, Frederico, WP, Ydrefors PRD 105, 114055 (2022)

We can calibrate the model to reproduce Lattice Data for $M(p^2)$

Phenomenological Model

Duarte, Frederico, WP, Ydrefors PRD 105, 114055 (2022)

We can calibrate the model to reproduce Lattice Data for $M(p^2)$



Set	\bar{m}_0 (GeV)	m_η (GeV)	Λ (GeV)	α
1	0.42	0.84	1.20	19.70
2	0.38	0.78	1.10	20.30
3	0.35	0.60	1.00	13.25

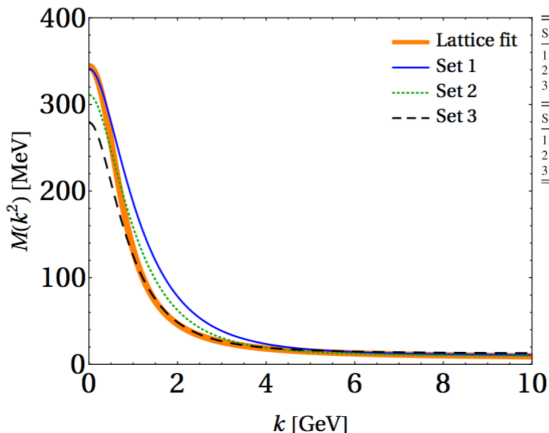
Set	(Outputs)	m_B (MeV)	R
1		9.06	2.22
2		8.53	2.09
3		12.25	2.64

Lattice data from: Oliveira, Silva, Skullerud and Sternbec, PRD 99 (2019) 094506

Phenomenological Model

Duarte, Frederico, WP, Ydrefors PRD 105, 114055 (2022)

We can calibrate the model to reproduce Lattice Data for $M(p^2)$



Set	\bar{m}_0 (GeV)	m_g (GeV)	Λ (GeV)	α
1	0.42	0.84	1.20	19.70
2	0.38	0.78	1.10	20.30
3	0.35	0.60	1.00	13.25

Set	(Outputs)	m_B (MeV)	R
1		9.06	2.22
2		8.53	2.09
3		12.25	2.64

Lattice data from: Oliveira, Silva, Skullerud and Sternbec, PRD 99 (2019) 094506

Next step: To use a solution of the DSE to obtain the **Fermion-Antifermion bound state**

Conclusions and Perspectives

- The near future will offer an innovative view of the dynamics inside the hadrons, thanks to the experimental activity planned at the Electron-ion colliders, and plenty of measurements pointing to the 3D tomography of hadrons will become available.
- For the pion, many results, em form factor, PDF, TMDs, Ioffe-time \times transverse plane distribution, have been obtained by using the ladder-approximation of the $q\bar{q}$ -BSE.
- The 3D imaging is in line with the goal of the future Electron Ion Collider.
- The pion has an important role, given its dual nature: $q\bar{q}$ bound-system and Goldstone boson. Our aim is to implement a framework analogous to the one already developed in Euclidean space.
- Minkowski space, phenomenological investigations, once the approach composed by BSE and gap-equations will be fully available, could offer fresh insights in hadron dynamics and possibly implement an interplay with well-established lattice and continuous QCD communities.